



Cite this: *Soft Matter*, 2018, 14, 7653

What causes the anomalous aggregation in pluronic aqueous solutions?†

Kuo-Chih Shih,^a Zhiqiang Shen,^b Ying Li,^b Martin Kröger,^c Shing-Yun Chang,^a Yun Liu,^{de} Mu-Ping Nieh^{id}*^{fg} and Hsi-Mei Lai^{id}*^a

Pluronic (PL) block copolymers have been widely used as delivery carriers, molecular templates for porous media, and process additives for affecting rheological behavior. Unlike most surfactant systems, where unimer transforms into micelle with increased surfactant concentration, anomalous large PL aggregates below the critical micelle concentration (CMC) were found throughout four types of PL (F108, F127, F88 and P84). We characterized their structures using dynamic light scattering and small-angle X-ray/neutron scattering. Molecular dynamics simulations suggest that the PPO segments, though weakly hydrophobic interaction (insufficient to form micelles), promote the formation of large aggregates. Addition of acid or base (e.g. citric acid, acetic acid, HCl and NaOH) in F108 solution significantly suppresses the aggregate formation for up to 20 days due to the repulsion force from the attached H₃O⁺ molecules on the EO segment in both PEO and PL and the reduction of CMC through the salting out effect, respectively.

Received 28th May 2018,
Accepted 21st August 2018

DOI: 10.1039/c8sm01096j

rsc.li/soft-matter-journal

Introduction

Poloxamers, also known as Pluronics[®] (PLs), are a series of triblock copolymers composed of polyethylene oxide–polypropylene oxide–polyethylene oxide (PEO–PPO–PEO) in different weight ratios of PEO and PPO segments.¹ PLs have been widely used for drug delivery,^{2–7} gene delivery,^{8,9} bioprocessing,¹⁰ fabrication of mesoporous materials^{11–13} and in other different kinds of fields. Many of these applications involve the use of PL micelles, where the concentration of PL is higher than the critical micelle concentration (CMC), the specific minimum concentration for surfactants to form micelles.^{14,15} PL micellization is driven by

the hydrophobic interaction between PPO segments shielded by a PEO layer composed of both ends of the PL in aqueous solution.¹⁶ The sizes of PL micelles range from a few to tens of nanometers depending on the molecular weights and the configurations of the PLs.^{17–20} Generally speaking, the micellar size is quite uniform and it is dictated by the spontaneous curvature of the PL molecules, which can be expressed by the “packing parameter”.²¹

In the past, the so-called “anomalous micellization” at a concentration prior to CMC has been reported in block copolymer systems,²² including PLs.^{23,24} The phenomenon was considered to be induced by the polydispersity of the PLs^{25–27} or the impurities in the system.^{28–31} Other than PLs, anomalous large aggregates that disappear upon increasing concentration have also been reported in other PEO-containing Gemini surfactants.³²

Anomalous aggregation has also been observed in PEO homopolymer aqueous solutions.^{33–36} Different hydrophobicities of the PEO backbone were proposed to explain the anomalous aggregation.^{33,34} A SANS study suggested that different end groups of the PEO homopolymer (hydroxyl or methoxy) resulted in different aggregation behaviors due to their hydrophobicity.³⁵ In addition, the sample preparation methods including the choice of solvent and heating history also play a role in the anomalous aggregation behavior.^{33,37} Most recently, a dynamic light scattering (DLS) study on multi-pass filtered PEO solutions, where the air bubbles are completely removed, indicated that the so-called large aggregates were air bubbles stabilized by PEO at the air–water interface.³⁸ This evidence implies that the

^a Department of Agricultural Chemistry, National Taiwan University, Taipei, 10617, Taiwan. E-mail: hmlai@ntu.edu.tw; Fax: +886-2-23633123; Tel: +886-2-33664816

^b Department of Mechanical Engineering, University of Connecticut, Storrs, Connecticut 06269, USA

^c Department of Materials, Polymer Physics, ETH Zürich, CH-8093 Zurich, Switzerland

^d Center for Neutron Research, National Institute of Standards and Technology, Gaithersburg, Maryland 20899, USA

^e Chemical & Biomolecular Engineering Department, University of Delaware, Newark, DE 19716, USA

^f Polymer Program, Institute of Materials and Science, University of Connecticut, Storrs, Connecticut 06269, USA. E-mail: mu-ping.nieh@uconn.edu; Tel: +1-8604868708

^g Department of Chemical and Biomolecular Engineering, University of Connecticut, Storrs, Connecticut 06269, USA

^h Department of Biomedical Engineering, University of Connecticut, Storrs, Connecticut 06269, USA

† Electronic supplementary information (ESI) available. See DOI: 10.1039/c8sm01096j

formation of large aggregates in PL solutions could also be attributed to “air bubbles”. Furthermore, the report also indicated that an increase of the solution salinity may enhance the formation of PEO aggregates.

Our previous study on a multicomponent system of PL/citric acid aqueous solution also revealed large aggregates³⁹ while the origin of the observed anomalous aggregation was difficult to identify due to the complexity of the system. In the current work, we focus on bare pluronic solutions and monitor the system under different processes to understand the birth of these large aggregates, and the effects of introduced air (by agitation) and salinity (acid, base or ions) on the aggregation rate, with a focus mainly on the F108 system.

Experimental section

Materials

Pluronic (PL) F108 (EO₁₃₃-PO₄₉-EO₁₃₃, M_w 14 600 g mol⁻¹), F88 (EO₁₀₃-PO₃₉-EO₁₀₃, M_w 11 400 g mol⁻¹), F127 (EO₁₀₁-PO₅₆-EO₁₀₁, M_w 12 600 g mol⁻¹) and P84 (EO₁₉-PO₄₄-EO₁₉, M_w 4200 g mol⁻¹) were obtained from BASF (Florham Park, New York, USA). Citric acid (CA), hydrochloric acid (HCl), acetic acid (Ace), sodium chloride (NaCl) and sodium hydroxide (NaOH) were purchased from Sigma-Aldrich (St. Louis, MO, USA).

Preparation of pluronic solutions

PL solutions were prepared by dissolving various amounts of PL in filtered solvents and storing at 6 ± 2 °C for 12 h in order to fully dissolve the PLs. These PL solutions were stored at 25 °C for another 24 h before taking measurements. For F108, 1, 5 and 8% (mass fraction) polymer solutions were prepared. For F127, a 0.5% (mass fraction) polymer solution was made while 1% (mass fraction) polymer solutions were prepared for F88 and P84. In the rest of the study, all the polymer concentrations will be expressed by mass fraction.

Nuclear magnetic resonance (NMR) spectroscopy

The ¹³C NMR data were acquired using a Bruker Advance-500 MHz FT-NMR spectrometer (500 MHz), operating at 125.76 MHz for ¹³C. The ¹³C NMR experiments were performed at 298 K using a delay of 2 s between pulses (pulse width 10.0 μs), and a sweep width of 34 090 Hz. The spectra were processed and analyzed by TopSpin 3.0. 10 wt% F108, F88, F127 and P84 samples were prepared in D₂O.

Dynamic light scattering (DLS)

The light scattering instrument is an ALV compact goniometer system with multi-detectors (CGS-3MD) (Germany), which consists of a 22 mW He-Ne laser (wavelength(λ) = 632.8 nm) and four avalanche photo diode detectors, which are equally spaced out (each 32° apart). One of the four detectors has a sample and a reference output, allowing pseudo-cross correlation measurements (single detector mode), thus yielding better data quality in the range of fast decay time (τ). The autocorrelation function was collected using an ALV-7004 digital multiple tau real

time correlator. In this experiment, the DLS data were obtained from the cross-correlation function in single detector mode. For the single-sized system, the intensity correlation function, $g_1(\tau)$, can be described as a single exponential decay, $e^{-\Gamma\tau}$, where Γ is the decay rate. As a result, the translational diffusion coefficient, D , can be related with Γ by a simple function, $D = \Gamma/q^2$, where the magnitude of the scattering vector is $q \equiv \frac{4n\pi}{\lambda} \sin \frac{\theta}{2}$ with n being the refractive index of the solution and λ is the incident laser wavelength (= 632.8 nm). In this report, the scattering angle, θ , was always set at 90°. Based on the Stokes-Einstein relation, the hydrodynamic radius, R_H , can be related with D of a uniform-sized spherical particle *via* $R_H = k_B T / 6\pi\eta D$, where k_B and η are the Boltzmann constant and the viscosity of the solvent (H₂O in this case), respectively. If the system contains more than one size of particles, the time correlation function indicates multimodal decays deviating from the single exponential decay. The ALV software is able to resolve multimodal distribution functions yielding multimodal distributions of R_H through the CONTIN procedure. The R_H histograms were plotted based on the intensity-weighted outcome.

Small-angle X-ray scattering (SAXS)

The samples were loaded in quartz capillary tubes and sealed. Small-angle X-ray scattering (SAXS) measurements were conducted on a Bruker Nano STAR instrument. Cu-K_α X-ray with the wavelength (λ) of 1.5418 Å was generated by a Turbo (rotating anode) X-ray source (TXS). The 2-D intensity data were collected using a Mikro Gap VANTEC-2000 detector (pixel size = 67 μm) with a sample-to-detector distance of 107.5 cm to cover a scattering vector, q (with $n = 1$), ranging from 0.007 to 0.21 Å⁻¹. Both scattering and transmittance of each sample were measured separately. The 2D raw data were corrected by the sample transmission, empty cell scattering and transmission. The corrected data were then circularly averaged, yielding the 1-D profiles.

Small-angle neutron scattering (SANS)

SANS experiments were conducted at NGB 30 m SANS at National Institute of Science and Technology (NIST), center for Neutron Research (NCNR, Gaithersburg, MD). Access to NGB 30 m SANS was provided by the Center for High Resolution Neutron Scattering (CHRNS), a partnership between the NIST and the National Science Foundation (NSF) under Agreement No. DMR-1508249. The SANS data were collected at two different sample-to-detector distances (7 and 4 m) with neutrons that have an average wavelength of 6 Å and a spread of 12.5%. This yielded a q range of 0.006 to 0.32 Å⁻¹. The 2-D raw data were collected and corrected for detector sensitivity, background, sample transmission, empty cell scattering and transmission. The corrected data were then circularly averaged, yielding the 1-D profiles, which were then put on an absolute intensity scale using the measured incident beam flux.

Small-angle scattering data analysis

Both SAXS and SANS data were analyzed using SasView 4.1.⁴⁰ This work was originally developed as part of the DANSE project

funded by the US NSF under Award DMR-0520547, but it is currently maintained by a collaboration between UTK, UMD, NIST, ORNL, ISIS, ESS, ILL and ANSTO. SasView also contains code developed with funding from the EU Horizon 2020 research and innovation programme under the SINE2020 project (Grant No. 654000). The scattering patterns were fitted by combining a low q power law and a Gaussian chain. The equation is listed as follows.

$$I(q) = Aq^{-\alpha} + BI_0P(q) + \text{BKG}, \quad (1)$$

where

$$I_0 = \varphi_{\text{poly}} V (\rho_{\text{poly}} - \rho_{\text{sol}})^2, \quad P(q) = \frac{2[\exp(-x) + x - 1]}{x^2},$$

$$x = q^2 \langle R_g^2 \rangle \text{ and } V = \frac{M_W}{N_A \delta}$$

Here, $P(q)$ is the Debye function. A and B are the scale factor for the two terms, respectively. φ_{poly} is the volume fraction of the polymer, V is the molecular volume of a polymer coil, δ is the density of the molecules, ρ_{poly} and ρ_{sol} are the neutron scattering length densities (nSLDs) or the X-ray scattering length densities (electron densities) of the polymer and solvent, respectively, and $\langle R_g^2 \rangle$ is the mean square radius of gyration of the PL. M_W is the weight-average molecular weight of the polymer, N_A is Avogadro's number and BKG is the incoherent background.

Molecular dynamics simulation

Due to the limited approachable time and length scales of all-atom molecule dynamics (MD) simulations, computational studies based on atomistic resolved models are restricted to single chain systems.^{41,42} To this end, coarse-grained models provide the best compromise between accuracy and efficiency. In this work, MARTINI based coarse-grained MD simulations were used to investigate the behaviors of PLs in aqueous solution. The MARTINI model provides a powerful tool to study the problems concerning lipids, proteins and polymers due to its ability to capture their chemical properties at a moderate computational cost^{43,44} In our simulations, the standard MARTINI water model was used, where each water bead represents four water molecules. The PL model was adopted from a previous study,⁴⁵ in which each monomer of PEO or PPO is coarse-grained into a single bead. Bonds, angles and Lennard-Jones (LJ) interaction parameters in this coarse-grained model are calibrated based on all-atomistic simulation results and reproduce their known $\langle R_g^2 \rangle^{1/2}$ and end-to-end distance.

To obtain the initial configurations of the well-dispersed polymers in all simulations, the PLs were firstly treated as pure PEO chains and relaxed under the NPT ensemble at temperature $T = 300$ K and pressure $P = 1$ bar. Subsequently, the beads in the middle part of certain chains were converted to PPO to investigate their aggregation behaviors. To explore PLs at an air–water interface, simulation boxes were extended along one (the z) direction. A time step of 20 fs was taken in all simulations. All the beads in our simulation shared the same constant mass of 72 amu for efficiency. All the coarse-grained MD

simulations were performed by using the Large-scale Atomic/Molecular Massively Parallel Simulator (LAMMPS) package.⁴⁶

To quantify the amount of PL aggregates at each time step, we employed a distance criterion based on the coordinates of the centers of masses of all the central PPO fragments. Each pair of polymers belongs to the same aggregate, if the distance between their PPO fragments, subject to periodic boundary conditions, is below 20 Å. Individual polymers not belonging to any such aggregate are denoted as 1-aggregate. The distance was chosen as it is large compared with the $\langle R_g^2 \rangle^{1/2}$ of an individual PPO fragment and small compared with the distance between the polymers in a homogeneous situation. Simulation results do not qualitatively depend on the choice of the critical distance for the aggregate analysis if these inequalities are met. From the amount of n -aggregates, we have access to the mean number of polymers forming an aggregate ('mean aggregate size') or the number of chains in true aggregates of size larger than unity. For each aggregate, we calculated a gyration tensor using the coordinates of all monomers belonging to the participating polymers and a mean gyration tensor by an arithmetic average over the aggregates. $\langle R_g^2 \rangle^{1/2}$ (square root of its trace) characterizes the spatial extension of the aggregates. It should be noted that LAMMPS was performed on F88 to reduce the cost of simulation time.

Thermal gravimetric analysis (TGA)

TGA measurements were conducted on a thermo-gravimetric analyzer (Q500, TA instrument, New Castle, England). 1% F108 original and centrifuged upper and lower layer solutions were dried individually in the sample pan to reach ~ 10 mg for the TGA measurements. The samples were heated in a furnace injected with N_2 (60 mL min^{-1}) at a heating rate of $5 \text{ }^\circ\text{C min}^{-1}$, from 25 to $700 \text{ }^\circ\text{C}$. The residual weight percentage (wt%, on dry basis) was recorded as a function of temperature.

Gel permeation chromatography (GPC)

1% F108 original and centrifuged upper and lower layer solutions were diluted to 0.1% (w/v) for the GPC analysis. A Waters Ultrahydrogel™ 250 column [$7.8 \text{ mm (ID)} \times 300 \text{ mm (L)}$], which was packed with crosslinked hydroxylated polymethacrylate-based gels of 250 Å pore size, was used. Filtered H_2O with 0.05% NaN_3 was used as the eluent. The columns were kept in a column oven at $40 \text{ }^\circ\text{C}$ and the flow rate was 0.5 mL min^{-1} . A refractive index detector was used and set to $35 \text{ }^\circ\text{C}$ to determine weight molecular size distributions.

Results and discussion

Large F108 aggregates

Fig. 1(a) shows the autocorrelation functions of 1, 5 and 8% F108 in H_2O using DLS measurements. All of them display composite curves composed of multiple exponential decays, indicating the coexistence of both slow (corresponding to large aggregates) and fast (corresponding to small aggregates) modes in the F108 solution. In fact, such a phenomenon was also

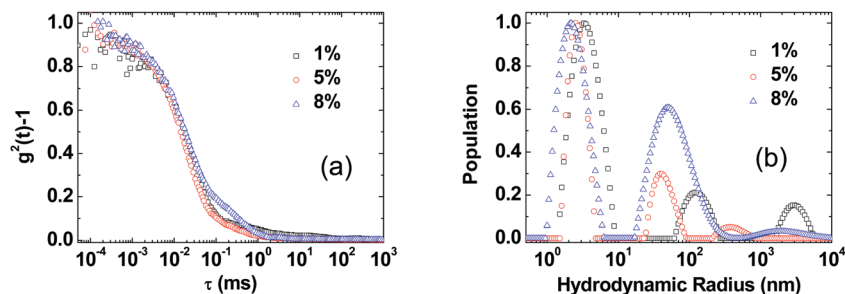


Fig. 1 Autocorrelation functions (a) and R_H histograms (b) of 1 (black square), 5 (red circles) and 8% (blue triangles) PL F108 in H_2O .

found in F127, F88, and P84 solutions (Fig. S1, ESI[†]), suggesting that this may be relatively common in PLs. Histograms of the deduced hydrodynamic radius (R_H) are presented in [Fig. 1(b)]. The general feature for the histogram of R_H includes three populations with peak positions located at 2–3 nm, 40–150 nm, and beyond 400 nm, respectively. The first peak reveals a consistent size with that of the F108 unimers, as reported from the SANS measurement ($\langle R_g^2 \rangle^{1/2} = 2.3$ nm).⁴⁷ The second population of aggregates in the 5 and 8% samples represents most likely the F108 polymeric micelles, as the critical micelle concentration (CMC) of F108 was reported to be 4.5% at 25 °C.⁴⁸ For the 1% sample, the existence of the second population was unexpected. The population with the largest radius may potentially be related to aggregates induced by impurities²⁷ or air bubbles.³⁸ In order to understand the origin of the PL aggregation mechanism, we chose to investigate 1 and 5% F108 (one above and one below its CMC).

According to a previous study,³³ centrifugation could separate the large PEO aggregates from the unimers in aqueous solutions. After F108 solutions were centrifuged at 15 000g for 30 min, no sediment was found and both upper and lower layer solutions were transparent with no clear boundary. We then performed DLS and SAXS measurements on the upper half of the solution. Fig. 2(a) and (b) show the autocorrelation functions and the corresponding histograms of R_H of the upper half solutions of the centrifuged 1 and 5% F108 samples, respectively. The size distribution function [Fig. 2(b)] confirms that the large aggregates (>100 nm) of impurity were completely removed. Instead, unimers (~ 3 nm) remained for both solutions (1 and 5%) while some micelles (~ 40 nm) were also found only in the 5% solution. This evidence implies that the chosen centrifugal condition was sufficient to spin down the aggregates with $R_H > 100$ nm. In contrast, the autocorrelation functions and R_H histograms [Fig. S2(a) and (b), ESI[†]]

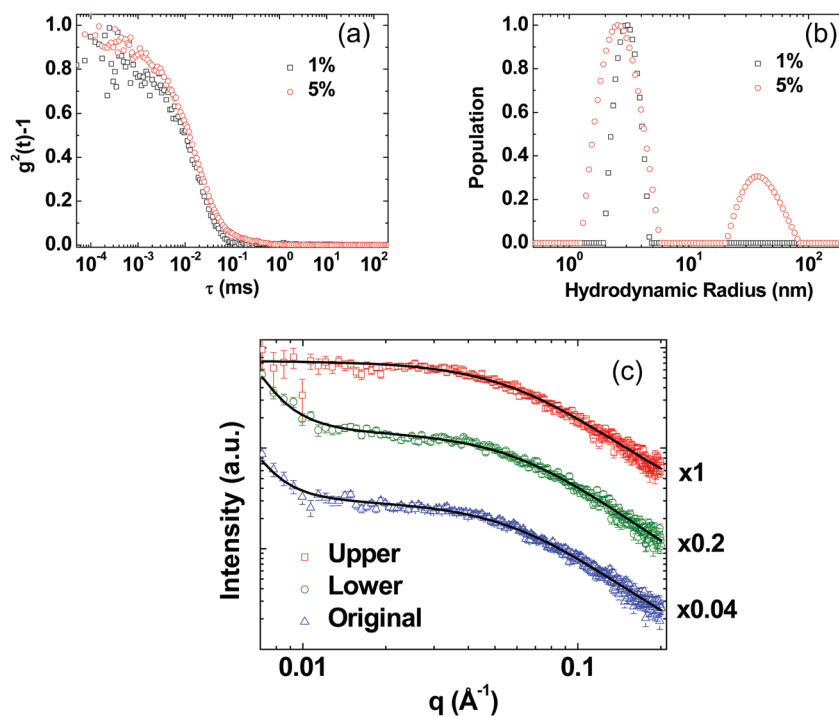


Fig. 2 Autocorrelation function (a) and R_H histogram (b) for the upper layer solution of 1 (black square) and 5% (red circle) F108 after centrifugation. SAXS results for the upper (red square) and lower (green circle) layer solutions after centrifugation and the original solution (blue triangle) of 5% F108 (c). The solid lines represent the best fitted results by using eqn (1).

of the lower half solutions indicate that the large aggregates remained.

The SAXS data of the 5% F108 solutions (original, centrifuged upper half and centrifuged lower half) [Fig. 2(c)] were also consistent with the DLS observations. The scattering curves were practically identical to the data above $q = 0.01 \text{ \AA}^{-1}$ and can be best fitted using a combination of a power law decay (large aggregates) with a Gaussian polymer chain (unimer) model, as expressed in eqn (1),⁴⁷ yielding $\langle R_g^2 \rangle^{1/2} = 2.6 \text{ nm}$. In a previous study,⁴⁹ $R_H = 0.853 \langle R_g^2 \rangle^{1/2}$ for hydrated PEO homopolymer. Therefore, R_H and $\langle R_g^2 \rangle^{1/2}$ are in good agreement. However, differences between various samples were found in the initial low q slope. An intensity plateau was only observed for the centrifuged upper half solution, indicating that there were no detectable large aggregates within the probing range. However, for the original solution and lower half solution after centrifugation, an intensity upturn with a q^{-4} decay was observed at $q < 0.01 \text{ \AA}^{-1}$, presumably a scattering tail stemming from an unattainable lower q regime, suggesting both solutions contained large aggregates, consistent with the DLS outcomes.

The time-resolved study on the centrifuged upper half solutions of 1 and 5% F108 gives an intriguing outcome. At least two decays were found in both autocorrelation functions obtained from the upper half solutions after 2 days of storage time [Fig. 3(a)], corresponding to multi-modal size distribution functions [Fig. 3(b)]. The large aggregates ($> 100 \text{ nm}$) reappeared and coexisted with the PL unimers ($\sim 3 \text{ nm}$) for the 1% sample, and both unimers and micelles ($\sim 40 \text{ nm}$) in the case of the 5% sample. The SAXS data of all three 5% PL samples (original, centrifuged upper half and centrifuged lower half) exhibit a

low- q intensity upturn after 2 days of storage [Fig. 3(c)], indicative of the existence of large aggregates – in good agreement with the DLS data. The q^{-4} Porod scattering at low q also suggests that the size of such aggregates was beyond the SAXS probing range. This observation reveals two facts. Firstly, the large aggregates (with $R_H > 100 \text{ nm}$) indeed form spontaneously in the F108 solutions at a concentration lower than CMC even after they are removed from the solution. Secondly, the density of the aggregates is higher than that of water since they are concentrated at the lower part of the solution after centrifugation.

The origin of the large aggregates

A careful investigation on PEO solution reported that air bubbles stabilized by the PEO at the air/water interface are the cause of the observed aggregates.³⁸ The question is whether the formation mechanism of the PL aggregates is the same as that of the PEO aggregates, *i.e.*, stabilized air bubbles. In order to identify the mechanism, air was purged into the centrifuged upper half solution, where no aggregates were initially observed [as shown in Fig. 2(b)], under vigorous agitation for 3 h. Afterwards, re-centrifugation was applied to the solution and the upper half and lower half solutions were collected individually. Both DLS and SANS measurements were again conducted on the following three samples: agitated upper half solution after centrifugation, the upper half and lower half solutions after re-centrifugation. Fig. 4(a) and (b) illustrate the autocorrelation functions and the histograms of R_H of these three samples. Indeed, large aggregates, whose sizes (from 60 nm to above micron) resembled the spontaneous forming aggregates after 2 days of storage, clearly reappeared, after vigorous agitation.

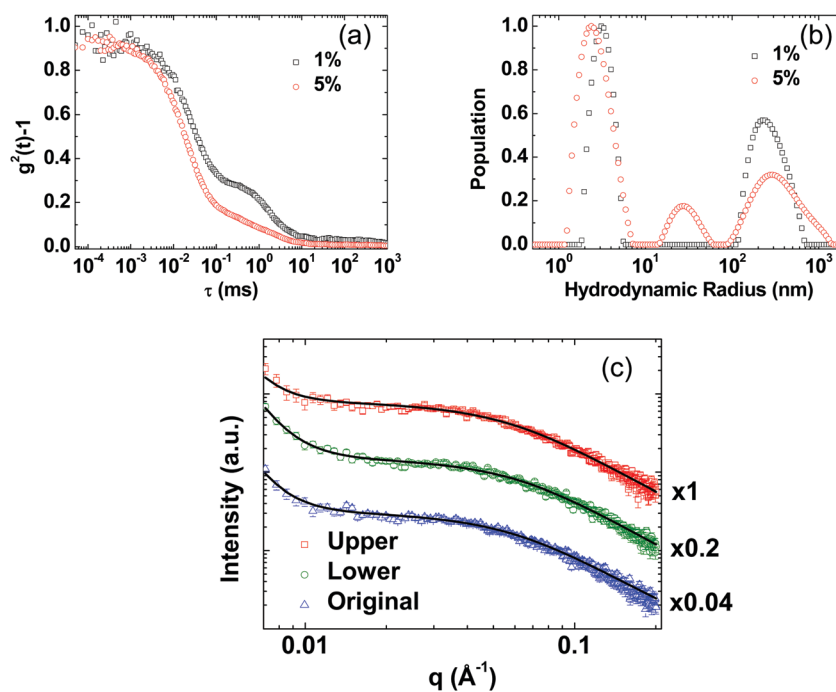


Fig. 3 Autocorrelation function (a) and R_H histogram (b) for the upper layer solution of 1 (black square) and 5% (red circle) F108 after two-days of storage. SAXS results for the upper (red square), lower (green circle) layer solution and the original solution (blue triangle) of 5% F108 after two-days of storage (c). The solid lines represent the best fitted results by using eqn (1).

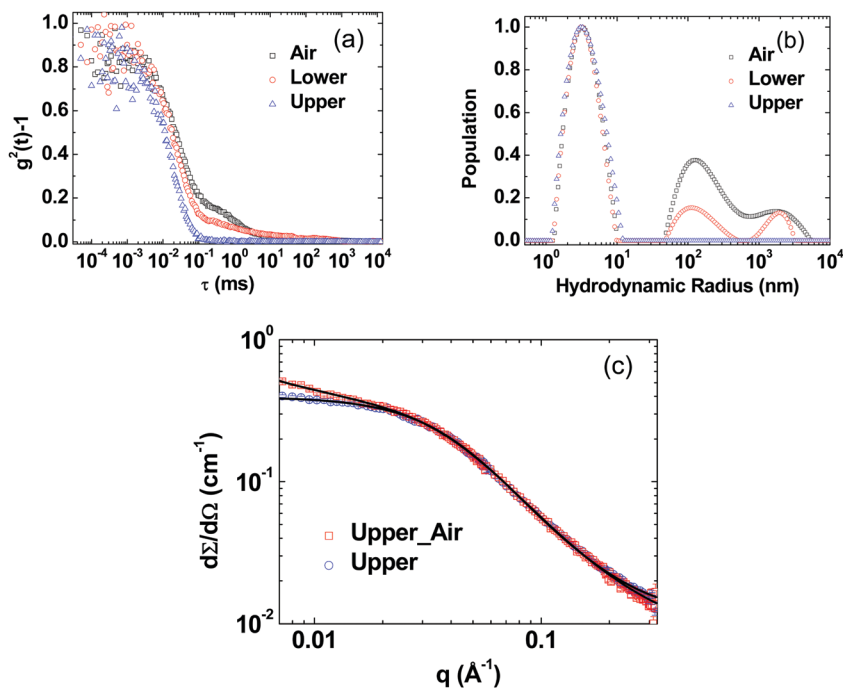


Fig. 4 Autocorrelation functions (a) and R_H histograms (b) of the 1% F108 air introduced (black squares) solution, and the lower (red circles) and upper layer (blue triangles) solutions after re-centrifugation of the agitated sample. The SANS data for the upper layer solution after removing aggregates (blue circles) and the air-introduced upper layer solution sample (red squares) (c). The solid lines represent the best fitted results by using eqn (1).

The F108 aggregates can also be observed in the SANS data measured from the agitated sample and the re-centrifuged upper half solution illustrated in Fig. 4(c), which show practically two identical SANS curves at $q > 0.02 \text{ \AA}^{-1}$, corresponding to the scattering of F108 unimers but with a notable difference in the low- q regime (*i.e.*, $< 0.01 \text{ \AA}^{-1}$). The evident increase of the low- q intensity observed in the agitated sample in contrast to the plateau intensity found in the re-centrifuged upper half solution [the best fitted $A = 0$ in eqn (1)] suggests that agitation results in large aggregates with a density higher than water. Here, the best fit of the low- q power-law exponent was -2.3 , instead of -4 observed in the centrifuged sample left for 2 days, suggesting that the aggregates caused by vortexing might be fractal and smaller. To further investigate the composition of the aggregates, contrast-matching SANS was performed on the agitated sample and the centrifuged lower solution after agitation in $\text{H}_2\text{O}/\text{D}_2\text{O}$ solvent whose nSLD matches with that of the pluronic (Fig. S3, ESI†). No detectable coherent scattering was observed in the probing q range for both samples, suggesting that the major composition of the aggregates is presumably F108 instead of air bubbles, whose nSLD is drastically different from that of the solvent. Both this outcome and the aforementioned higher density of the aggregates than water indicate that the formation mechanism of PL aggregates may be different from that of the stabilized air bubbles in the PEO solution.³⁸ One of the possible mechanisms is that the introduced air bubbles act as aggregating “seeds” to attract the PPO of PL and thus consequently induce the PL aggregation. The other would be an enhanced collision frequency between PL *via* agitation. Since this proposed mechanism is difficult to verify experimentally,

molecular dynamics (MD) simulation was performed on P84 (Fig. S4, ESI†). No polymer aggregate was observed at the air-water interface. While doubling the P84 concentration to explore the effect of PL concentration, a similar result could also be obtained. We further increased the PPO segment length for PLs in solution to investigate the influence of the PPO segment length. However, it was found that the enlarged PPO segment length promotes the formation of PL micelles instead of the aggregation of PPO at the air/water interface. Moreover, this proposed mechanism does not support the fact that the aggregation rate of more hydrophilic PL was the same as, if not faster than, those of the more hydrophobic ones.

It is noteworthy that both TGA [Fig. S5(a), ESI†] and GPC results [Fig. S5(b), ESI†] suggest that there are impurities, presumably PEO homopolymer, as previously reported,⁴⁹ in the F108 solution that cannot be completely removed by centrifugation. The ^{13}C NMR spectra (Fig. S6, ESI†) for all examined PLs also suggest that other carbon-related impurities are insignificant compared to the major functional groups of PEO and PLs. Therefore, the question remains: “*Is the anomalous aggregation induced by the PEO homopolymer in the F108 solution?*”

A detailed time-dependent MD simulation was performed on the behaviors of F88 with or without PEO homopolymers to investigate the initiation of aggregates. Here, the molecular weight of the PEO homopolymer was chosen to be 4500, as indicated by a previous study.⁵⁰ For comparison, two different systems with 100 polymer chains were built in a simulation box of $70 \times 70 \times 70 \text{ nm}^3$. Particularly, the first one contains 100 chains of F88 while the other one has 20 wt% PEO4500 in F88 with 100 chains in total. The polymer mass fraction in

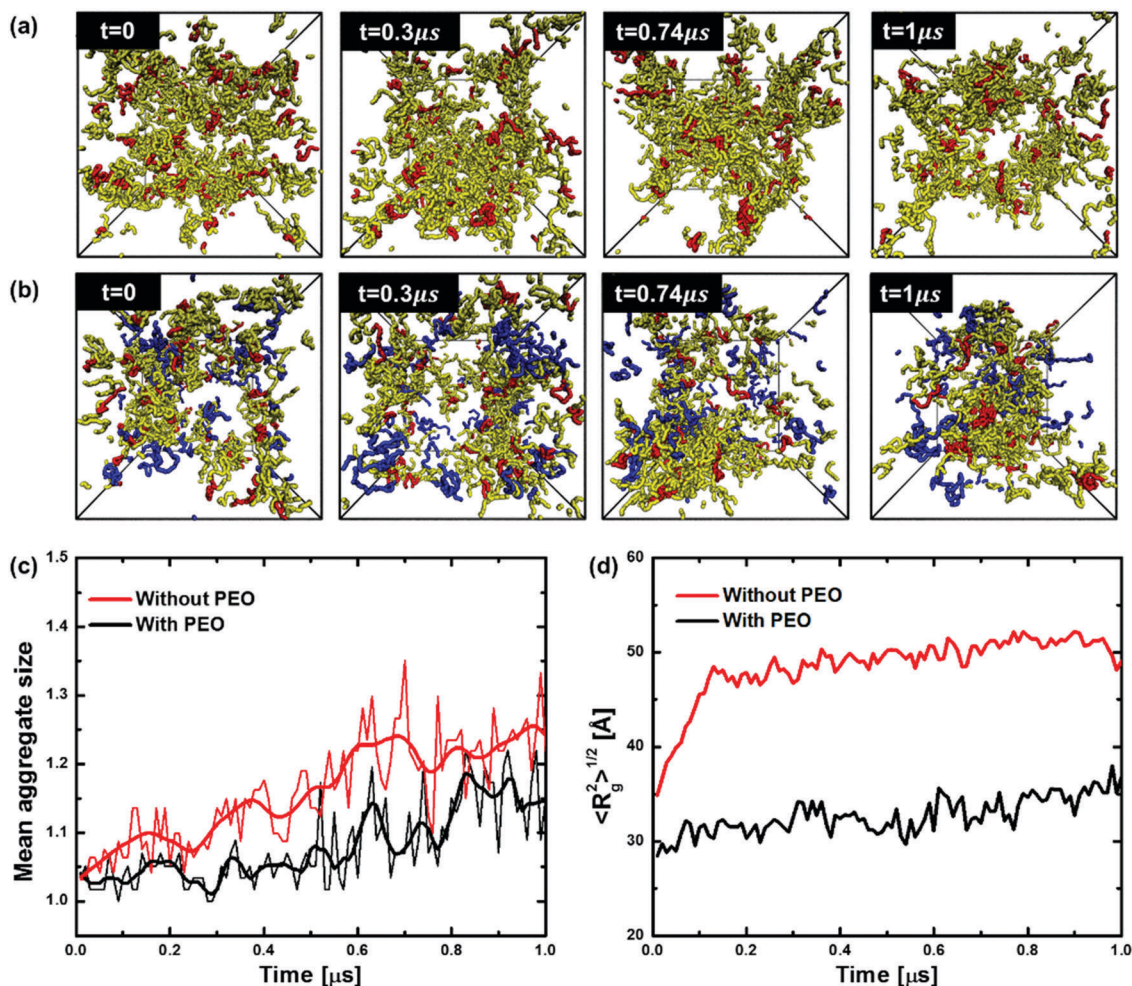


Fig. 5 MD simulation results on the aggregation behaviors of F88 without and with PEO4500, respectively. Snapshots of pure F88 systems (a) and PEO4500 systems (b); evolution of mean aggregate size (c) and radius gyration (d). Water beads are not shown for clarity. In the figures (a) and (b), the PPO part of F88 is colored in red, the PEO part of F88 is colored in yellow and the PEO4500 homopolymer is colored in blue.

these two systems was around 2 wt%, comparable to the experimental conditions. As shown in Fig. 5(a) and (b), all the polymers were initially randomly distributed in the simulation box. During the relaxation process of 1 μs , aggregations of F88 copolymers were found in both of the two systems, as shown at the time step of 1 μs . Specifically, as indicated in Fig. 5(c), the mean aggregate sizes of the two systems increase with the evolution of simulation time. In addition, with the formation of F88 aggregates, the R_g of polymers also increases [see Fig. 5(d)]. To further explore the details of the aggregation of F88, the dynamic process of a specific aggregate in systems shown in Fig. 5 was extracted and plotted in Fig. 6. As shown in Fig. 6(a), the F88 polymers are initially separated from each other at the time step $t = 0$. Due to the hydrophobicity of PPO, the PPO segment in each F88 chain tends to fold and collapse to reduce this contact area with water at $t = 0.3 \mu\text{s}$. A small aggregate with several F88 chains forms. However, because of the small hydrophobicity ratio in F88, the hydrophobic force of the PPO segment was not strong enough to form the micelle. Simultaneously, the relatively hydrophilic PEO moieties in the F88 chains start to

intercross with each other to connect these small aggregates. Finally, the F88 polymers form a bigger aggregate at $t = 1 \mu\text{s}$. A similar process was observed for the system with PEO4500, as shown in Fig. 6(b). The existence of the PEO homopolymer does not affect the formation of small aggregates caused by the collapse of PPO in F88, while the PEO homopolymer may act as a bridge to connect these aggregates. In addition, Fig. 7 shows the growth kinetic of aggregation on a longer time scale, indicating that both the quantity [Fig. 7 (a)] and size [Fig. 7 (b)] of the aggregates increase after 1.5 days of storage. Therefore, we propose that the hydrophobic interaction between the PPO segments is the initial force to form the aggregates, presumably independent of the PEO homopolymer. With increasing time, the size of these aggregates increases until they are detectable in the DLS measurement. The aforementioned agitation process simply enhances the probability of collision and bridging of aggregates with F108 unimers. It is noteworthy that once the large aggregates formed, either vortexing or addition of acids or bases would not dissociate them, as shown in Fig. S7 (ESI[†]).

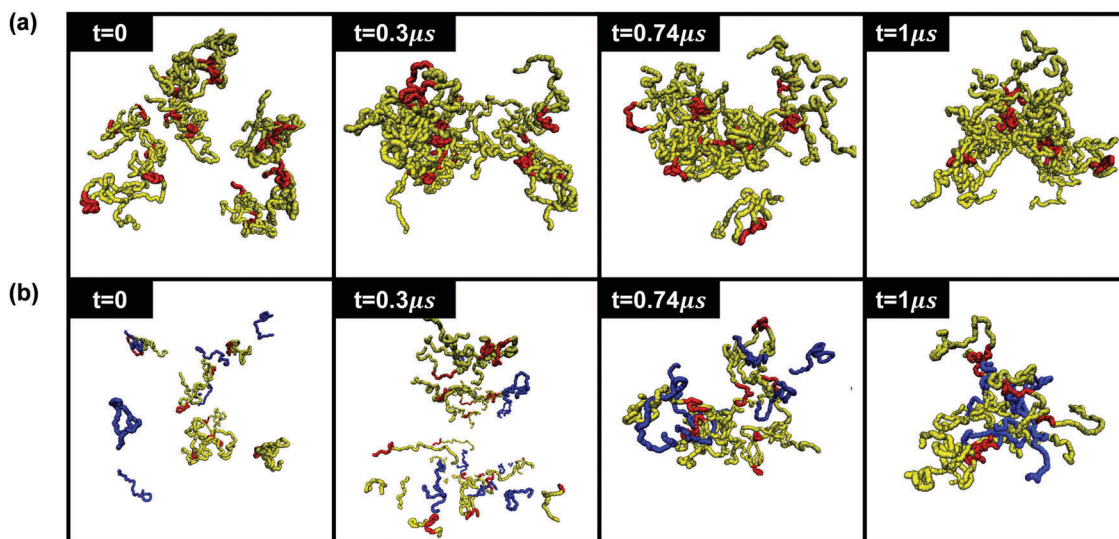


Fig. 6 The dynamics of a specific aggregate formed by several unimers (shown in Fig. 5), which are initially apart, without (a) and with PEO45000 (b). The PPO part of F88 is colored in red, the PEO part of F88 is colored in yellow and the PEO4500 homopolymer is colored in blue.

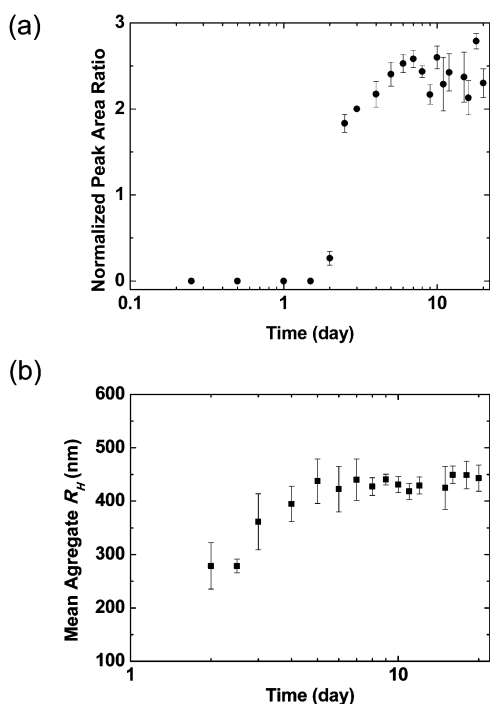


Fig. 7 F108 aggregation kinetics presented as the ratio of the peak area of the large aggregates to the F108 unimer obtained by the R_H histograms from the DLS measurements (a) and the aggregate size (considering above 100 nm) as a function of storage time (b).

We further investigated the effect of the solution salinity on the formation of the aggregates. The centrifuged aggregate-free upper half solutions were individually supplemented with citric acid (CA), acetic acid (Ace), hydrochloric acid (HCl), sodium chloride (NaCl) and sodium hydroxide (NaOH). The final concentration of these five components was fixed at 0.26 M. The autocorrelation functions and the histograms of R_H of the individual centrifuged upper half solutions right after the addition of

acid/base/salt are shown in Fig. 8(a) and (b), respectively. They are nearly identical except for the case of NaOH, whose decay of autocorrelation function is delayed, indicating the larger particles. This is presumably attributed to the fact that NaOH effectively dehydrates PL, leading to a lower CMC, as previously reported in Pluronic P84 and Tetroic 904 solutions.⁵¹ The “salting-out” effect through the addition of NaOH has also been reported in the PEO homopolymer⁵² and the alkyl polyglucoside system.^{53,54} After 2 days of storage, a clear feature of two decays was observed in the autocorrelation functions of the NaCl-containing and H₂O-alone samples [Fig. 8(c)], indicating the formation of large F108 aggregates. However, only unimers were observed in the rest of the samples [Fig. 8(c) and (d)]. In fact, even after 20 days, the unimers remained the major species for the solutions containing CA, Ace, HCl and NaOH while the population of the large aggregates in the NaCl added sample increased [Fig. 8(e) and (f)]. The possible mechanisms of retarding the formation of large aggregates from PLs were not expected to be the same for the acidic and basic solutions. First, the electron-rich ether group of the EO segment has the tendency of associating with protonated water molecules (H₃O⁺). Hence, the addition of acid enhances the charge density on the EO segment for both PEO and PL, thus resulting in the repulsion between the PL molecules and consequently reducing the contact frequency between the unimers and inhibiting the aggregate formation.⁵⁵ In addition, the anions with higher charge density have a better ability to form ion/water complexes, and thus decrease the hydration of the PL.⁵⁶ In the basic solution, the addition of NaOH in the PL solution decreases the CMC, as mentioned previously. The suppression of forming large aggregates was consistent with the fact that the large aggregates prefer to form in some PEO-containing amphiphiles prior to the formation of micelles, as reported previously.^{23,24,32} NaCl seems to have no effect on inhibiting the aggregation. The time-dependent autocorrelation functions and the R_H

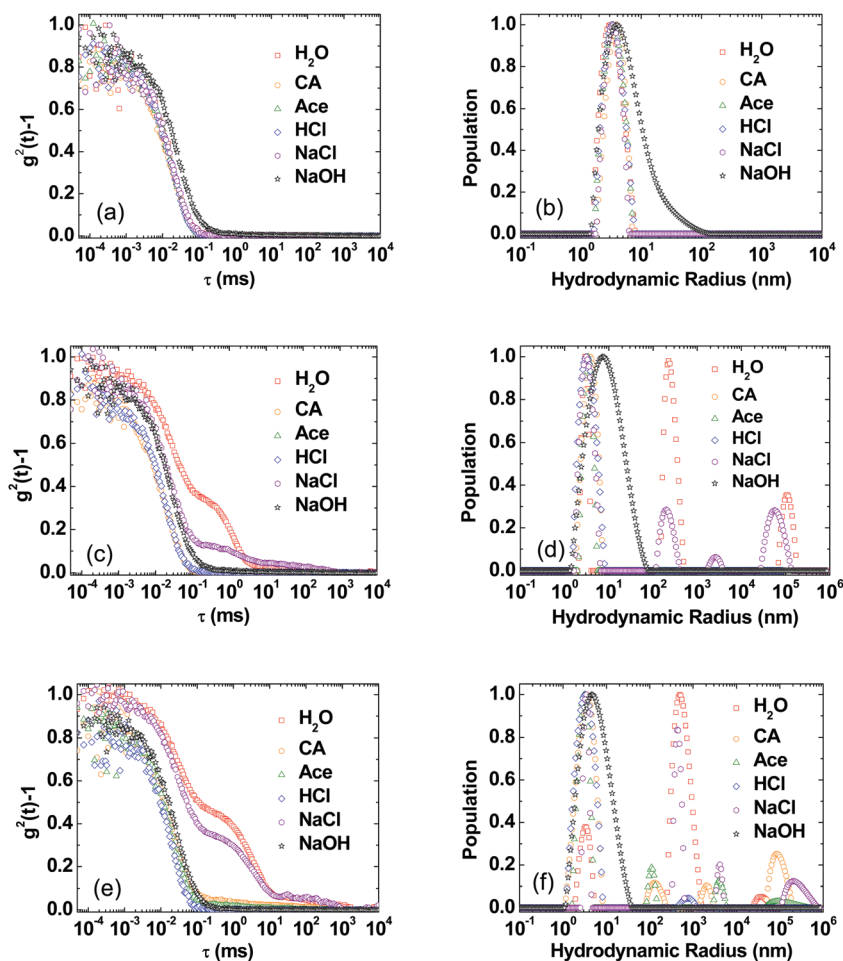
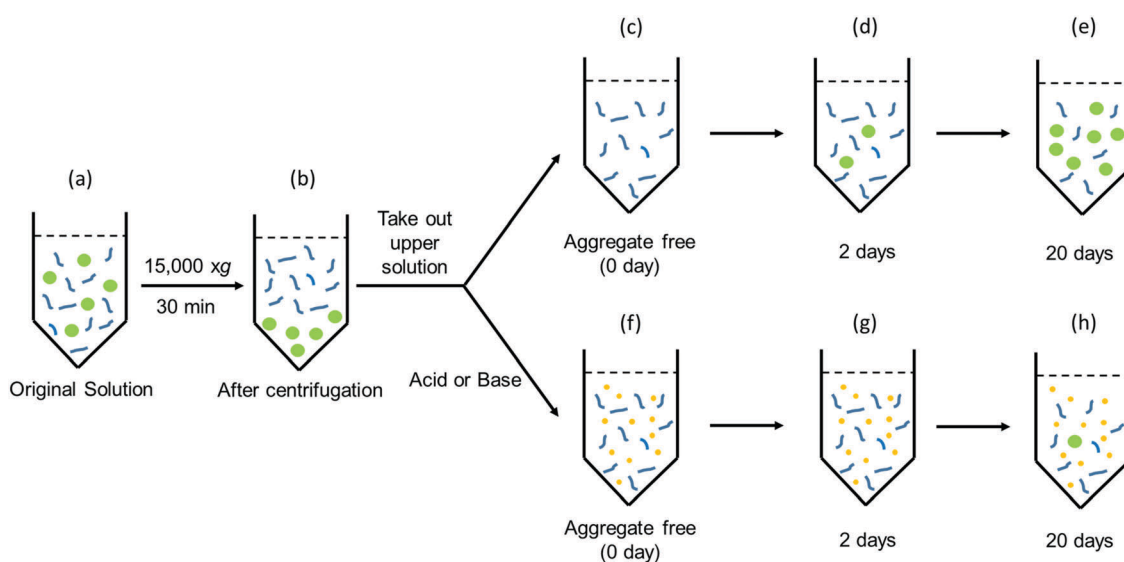


Fig. 8 Autocorrelation functions (a, c and e) and R_H histograms (b, d and f) of 1% F108 solution stored for 0 day (right after centrifugation) (a and b), 2 days (c and d) and 20 days (e and f) in H₂O (red squares), 0.26 M citric acid (orange circles), acetic acid (green triangles), HCl (blue diamonds), NaCl (purple hexagons) and NaOH (black stars) solutions.



Scheme 1 Schematic representation of the as prepared F108 solution (a) and after centrifugation (b). The upper half solutions without and with added salt are demonstrated in (c–e) and (f–h), respectively. Samples stored for 0, 2 and 20 days are presented in (c and f), (d and g) and (e and h). The blue, green and yellow colours represent PL unimers, anomalous aggregates and acidic/basic ions, respectively.

histograms of F127, F88 and P84 in both H₂O and CA solutions (Fig. S8–S10, ESI[†]) show consistent outcomes with those in F108 (suppressed aggregation by CA), confirming a similar aggregation mechanism.

Scheme 1 summarizes our experimental outcome. For 1% F108, anomalous aggregation (>100 nm) below the CMC is observed in the as prepared samples [Scheme 1(a)]. The large aggregates are denser than water (not likely to be air bubbles) and, therefore, they can be effectively separated by centrifugation [Schemes 1(b) and (c)]. The simulation result suggests that the weak hydrophobic interaction between the PPO segments leads to large aggregations, however, they are not strong enough to form micelles. Large aggregates reappear in the upper half solution after 2 days [Schemes 1(d) and (e)]. The formation of the aggregates can be inhibited by the addition of acids or bases [Schemes 1(g) and (h)]. Presumably, the repulsion force from complexing H₃O⁺ with the EO groups is likely the inhibition mechanism in the acidic solution, while the reduced CMC of F108 under the basic condition could be the other mechanism to inhibit the formation of large aggregates.

Conclusions

Large PL aggregates were observed in aqueous solutions prior to the CMC. These large aggregates have a higher density than that of water and can be effectively removed by centrifugation. They can reoccur over a period of time (~2 days). The MD simulations indicate that the PPO segments, though weakly hydrophobic (insufficient to form micelles), promote the formation of large aggregates. The aggregation rate can be effectively suppressed by either acids or bases. The current research outcome suggests a formation mechanism of the PL aggregates other than driven by air bubbles. This knowledge provides a fundamental understanding of the self-assembly behavior of PL.

Conflicts of interest

There are no conflicts to declare.

Acknowledgements

This work was supported by the Grant 102-2313-B-002-056-MY3 from the Ministry of Science and Technology (MOST), Taipei, Taiwan. The funding for the acquisition of the Bruker Nano-STAR instrument was partially supported by the National Science Foundation – Major Research Instrumentation grant (DMR 1228817). Certain commercial equipment, instruments, or materials (or suppliers, or software *etc.*) are identified in this paper to foster understanding. Such identification does not imply recommendation or endorsement by the National Institute of Standards and Technology (NIST), nor does it imply that the materials or equipment identified are necessarily the best available for the purpose.

References

- 1 P. Alexandridis and T. A. Hatton, *Colloids Surf., A*, 1995, **96**, 1–46.
- 2 L. Fang, L. Wang, Y. Yao, J. Zhang, X. Wu, X. Li, H. Wang, X. Zhang, X. Gong and J. Chang, *Nanomedicine*, 2017, **13**, 153–171.
- 3 L. M. Ensign, S. K. Lai, Y. Y. Wang, M. Yang, O. Mert, J. Hanes and R. Cone, *Biomacromolecules*, 2014, **15**, 4403–4409.
- 4 J. Wang, P. Gao, P. J. Wang, L. Ye, A. Y. Zhang and Z. G. Feng, *Polymer*, 2011, **52**, 347–355.
- 5 C. C. Perry, T. S. Sabir, W. J. Livingston, J. R. Milligan, Q. Chen, V. Maskiewicz and D. S. Boskovic, *J. Colloid Interface Sci.*, 2011, **354**, 662–669.
- 6 M. Yang, S. K. Lai, T. Yu, Y. Y. Wang, C. Happe, W. Zhong, M. Zhang, A. Anonuevo, C. Fridley, A. Hung, J. Fu and J. Hanes, *J. Controlled Release*, 2014, **192**, 202–208.
- 7 V. Sagar, S. Pilakka-Kanthikeel, R. Pottathil, S. K. Saxena and M. Nair, *Rev. Med. Virol.*, 2014, **24**, 103–124.
- 8 H. Song, S. Liu, C. Li, Y. Geng, G. Wang and Z. Gu, *Int. J. Nanomed.*, 2014, **9**, 3439–3452.
- 9 M. Yang, S. K. Lai, Y. Y. Wang, W. Zhong, C. Happe, M. Zhang, J. Fu and J. Hanes, *Angew. Chem., Int. Ed.*, 2011, **50**, 2597–2600.
- 10 D. W. Murhammer and C. F. Goochee, *Biotechnol. Prog.*, 1990, **6**, 391–397.
- 11 S. D. T. Barros, A. V. Coelho, E. R. Lachter, R. A. S. San Gil, K. Dahmouche, M. I. Pais da Silva and A. L. F. Souza, *Renewable Energy*, 2013, **50**, 585–589.
- 12 H. Liu, X. Sun, C. Yin and C. Hu, *J. Hazard. Mater.*, 2008, **151**, 616–622.
- 13 S. Soltani, U. Rashid, S. I. Al-Resayes and I. A. Nehdi, *Energy Convers. Manage.*, 2017, **141**, 183–205.
- 14 J. Grindley and C. R. Bury, *J. Chem. Soc.*, 1929, 679–684.
- 15 P. Muller, *Pure Appl. Chem.*, 1994, **66**, 1077–1184.
- 16 K. Mortensen, *EPL*, 1992, **19**, 599–604.
- 17 K. Mortensen and J. S. Pedersen, *Macromolecules*, 1993, **26**, 805–812.
- 18 O. Glatter, G. Scherf, K. Schillen and W. Brown, *Macromolecules*, 1994, **27**, 6046–6054.
- 19 G. Wanka, H. Hoffmann and W. Ulbricht, *Macromolecules*, 1994, **27**, 4145–4159.
- 20 K. Mortensen and W. Brown, *Macromolecules*, 1993, **26**, 4128–4135.
- 21 P. R. Cullis, M. J. Hope and C. P. S. Tilcock, *Chem. Phys. Lipids*, 1986, **40**, 127–144.
- 22 I. W. Hamley, *The Physics of Block Copolymers*, Oxford University Press, New York, 1998.
- 23 Z. Zhou and B. Chu, *Macromolecules*, 1988, **21**, 2548–2554.
- 24 Z. Zhou and B. Chu, *Macromolecules*, 1987, **20**, 3089–3091.
- 25 P. Lines, *Macromolecules*, 1994, **27**, 2685–2693.
- 26 P. Linse, *Macromolecules*, 1994, **27**, 6404–6417.
- 27 Y. H. Hsu, H. W. Tsui, S. Y. Ling and L. J. Chen, *Colloids Surf., A*, 2016, **509**, 109–115.
- 28 G.-E. Yu, H. Altinok, S. K. Nixon, C. Booth, P. Alexandridis and T. A. Hatton, *Eur. Polym. J.*, 1997, **33**, 673–677.

- 29 B. Trathnigg and A. Gorbunov, *Macromol. Symp.*, 2006, **237**, 18–27.
- 30 B. Trathnigg, *Polymer*, 2005, **46**, 9211–9223.
- 31 M. Nilsson, B. Håkansson, O. Söderman and D. Topgaard, *Macromolecules*, 2007, **40**, 8250–8258.
- 32 M. P. Nieh, S. K. Kumar, R. H. Fernando, R. H. Colby and J. Katsaras, *Langmuir*, 2004, **20**, 9061–9068.
- 33 M. Duval, *Macromolecules*, 2000, **33**, 7862–7867.
- 34 M. Duval and D. Sarazin, *Polymer*, 2000, **41**, 2711–2716.
- 35 B. Hammouda, D. L. Ho and S. Kline, *Macromolecules*, 2004, **37**, 6932–6937.
- 36 M. Polverari and T. G. M. Van De Ven, *J. Phys. Chem.*, 1996, **100**, 13687–13695.
- 37 P. C. Strazielle, *Makromol. Chem.*, 1968, **119**, 50–63.
- 38 J. Q. Wang, *Macromolecules*, 2015, **48**, 1614–1620.
- 39 K. C. Shih, C. Y. Li, W. H. Li and H. M. Lai, *Soft Matter*, 2014, **10**, 7606–7614.
- 40 M. e. a. Doucet, SasView Version 4.0, Zenodo, <http://doi.org/10.5281/zenodo.825675>.
- 41 S. Hezaveh, S. Samanta, G. Milano and D. Roccatano, *J. Chem. Phys.*, 2012, **136**, 124901.
- 42 S. Nawaz, M. Redhead, G. Mantovani, C. Alexander, C. Bosquillon and P. Carbone, *Soft Matter*, 2012, **8**, 6744–6754.
- 43 S. J. Marrink, H. J. Risselada, S. Yefimov, D. P. Tieleman and A. H. De Vries, *J. Phys. Chem. B*, 2007, **111**, 7812–7824.
- 44 S. J. Marrink and D. P. Tieleman, *Chem. Soc. Rev.*, 2013, **42**, 6801–6822.
- 45 S. Hezaveh, S. Samanta, A. De Nicola, G. Milano and D. Roccatano, *J. Phys. Chem. B*, 2012, **116**, 14333–14345.
- 46 S. Plimpton, *J. Comput. Phys.*, 1995, **117**, 1–19.
- 47 L. Fan, M. Degen, N. Grupido, S. Bendle and P. Pennartz, *Mater. Sci. Eng., A*, 2010, **528**, 127–136.
- 48 P. Alexandridis, J. F. Holzwarth and T. A. Hatton, *Macromolecules*, 1994, **27**, 2414–2425.
- 49 H. Lee, R. M. Venable, A. D. MacKerell and R. W. Pastor, *Biophys. J.*, 2008, **95**, 1590–1599.
- 50 H. J. Park and C. Y. Ryu, *Polymer*, 2012, **53**, 5052–5059.
- 51 R. Ganguly, Y. Kadam, N. Choudhury, V. K. Aswal and P. Bahadur, *J. Phys. Chem. B*, 2011, **115**, 3425–3433.
- 52 M. J. Hey, D. P. Jackson and H. Yan, *Polymer*, 2005, **46**, 2567–2572.
- 53 X. Jin, S. Zhang, J. Yang and R. Lv, *Tenside, Surfactants, Deterg.*, 2004, **41**, 126–129.
- 54 H. Y. Ji and M. Jie, *Maofang Keji*, 2010, **38**, 12–15.
- 55 B. Yang, C. Guo, S. Chen, J. H. Ma, J. Wang, X. F. Liang, L. Zheng and H. Z. Liu, *J. Phys. Chem. B*, 2006, **110**, 23068–23074.
- 56 R. Sadeghi and F. Jahani, *J. Phys. Chem. B*, 2012, **116**, 5234–5241.